Constraining dwarf spheroidal dark matter halos with the Galactic Center excess

Jeremie Choquette*

Department of Physics, McGill University, 3600 Rue University, Montréal, Québec, Canada H3A 2T8

(Received 29 August 2017; published 28 February 2018)

If the gamma-ray excess from the Galactic Center reported by Fermi-LAT is a signal from annihilating dark matter, one must question why a similar excess has not been observed in dwarf spheroidal galaxies. We use this observation to place constraints on the density profile of dwarf spheroidal galaxies under the assumption that the Galactic Center excess is in fact a signal from annihilating dark matter. We place constraints on the generalized Navarro-Frenk-White (NFW) parameter γ and the Einasto profile parameter α which control the logarithmic slope of the inner regions of the halo's density profile. The best-fit halo parameters R_s and ρ_s are determined using stellar kinematic data for a range of γ and α. We determine that under these assumptions the Galactic Center excess is inconsistent with the standard NFW profile (and other "cuspy" profiles) for dwarf spheroidal galaxies, but is consistent with observations of cored dwarf galaxy profiles. Specifically, we find that dwarf spheroidal profiles must be less cuspy than that of the Milky Way. Models of dark matter which self-interacts through a light mediator can achieve this.

DOI: 10.1103/PhysRevD.97.043017

I. INTRODUCTION

Observations by Fermi-LAT have indicated an excess of gamma rays in the center of the Milky Way galaxy in the range of a few GeV [1–9]. Interpretations of the Galactic Center excess (GCE) differ, with likely candidates including dark matter annihilations and known astrophysical phenomena. On the astrophysical side, the spectrum and morphology of the signal from millisecond pulsars provides a good fit to the observed excess [10–12], but this would require a much greater number of millisecond pulsars than are observed [13,14]. The Fermi-LAT Collaboration has more recently completed an analysis of the purported signal and has concluded that the morphology of the signal is more consistent with millisecond pulsars than with the dark matter interpretation [15,16]. It was concluded that the dark matter interpretation is strongly disfavored relative to other interpretations of the excess. In a recent paper, however, Haggard *et al.* argued that a sufficiently large population of millisecond pulsars would also imply a large population of observable low-mass x-ray binaries, limiting the contribution of millisecond pulsars to the Galactic Center excess to ∼4–23% [17], though it should be noted that these results are predicated on the assumption that the relative populations of low-mass x-ray binaries and millisecond pulsars are the same in the inner galaxy as in globular clusters. This nonetheless makes annihilating dark matter an interesting possibility.

It is also well known that there is tension between dark matter explanations of the Galactic Center excess and observations of dwarf spheroidal galaxies. Dwarf spheroidal galaxies show no corresponding signal, with the constraints seeming to exclude dark matter annihilation as a viable explanation for the Galactic Center excess [18,19]. The analysis of Ref. [18] (upon which Ref. [19] was based), however, assumed a Navarro-Frenk-White (NFW) profile for the dwarf spheroidals. The NFW profile has a sharp cusp at the center, leading to an enhanced signal relative to more "cored" dark matter distributions. We consider two profiles here: the generalized NFW profile and the Einasto profile, defined in Eqs. (3) and (4), respectively.

The exact distribution of dark matter in dwarf galaxies is not well known, but there is a large body of evidence pointing to cored profiles (see Sec. IV), or profiles with inner radii with slopes smaller than the $\rho \propto r^{-1}$ predicted by cold dark matter simulations and exemplified by the NFW profile.

The logarithmic slope of the inner dark matter halo can have a significant impact on its J-factor, a measure of the rate of dark matter annihilations within the halo. We will show that the tension between the dwarf galaxy observations and the GCE are reduced when considering more cored profiles. As the tension is moderate to begin with, it can be erased entirely for sufficiently cored profiles.

It also follows, therefore, that if the GCE signal were assumed to indeed originate from dark matter annihilations,

*jeremie.choquette@physics.mcgill.ca

constraints could be placed on the central slope of the dark matter profiles of the dwarf spheroidals. In Sec. II we simulate the GCE signal from dark matter to find best-fit values for the dark matter mass and annihilation cross section. In Sec. III we use these adopted values to place limits on the parameters γ and α which control how cuspy the dwarf spheroidals are. In Sec. IV we compare these values to those found through observation of dwarf spheroidals and simulations of cold dark matter (CDM) halos. In Sec. V we discuss the implications for the CDM paradigm, should the GCE prove to indeed be a signal from annihilating dark matter.

II. SIMULATION OF SIGNAL

It has been shown that the observed gamma-ray excess is well fit by models of annihilating dark matter in which the dark matter predominantly annihilates to $b\bar{b}$. The signal, however, consists of multiple components: the prompt gamma rays (from the b-decay products), inverse Compton scattering (ICS, caused by the upscattering of starlight and cosmic microwave background photons by the e^+/e^- produced as b-decay products), and a small amount of bremsstrahlung radiation (also from the decay products). These three sources combine to produce the total signal.

The prompt signal is easiest to compute numerically, as it depends only on the J-factor and average spectrum from a single annihilation, taken from PPPC 4 [20,21]:

$$\frac{d\Phi_{\text{prompt}}}{dE} = \frac{\langle\sigma v\rangle}{8\pi m_\chi^2}\frac{dN_\gamma}{dE} \times J, \tag{1}$$

$$J = \int_{\Delta\Omega}\int_{\text{l.o.s.}} \rho^2 dl d\Omega, \tag{2}$$

with the integral along the line of sight and angular extent of the observed system. The J-factor can then be computed numerically by assuming a density profile for the dark matter halo.

One way to parametrize the cuspiness of a galaxy is through the inner slope of the profile. If we assume a generalized NFW profile,

$$\rho(r) = \frac{\rho_s}{(\frac{r}{R_s})^\gamma(1+\frac{r}{R_s})^{3-\gamma}}, \tag{3}$$

then the parameter γ corresponds to the negative slope at $r = 0$. Larger values of γ correspond to a more cuspy profile, whereas smaller values correspond to a more cored profile. Following Ref. [6], we choose a generalized NFW profile with $R_s = 20$ kpc and $\rho_\odot = 0.40$ GeV cm^{-3} (the local dark matter density, which for $\gamma = 1$ corresponds to a scale density of $\rho_s = 0.26$ GeV cm^{-3}).[1] γ is typically taken to be somewhere on the order of 1.0–1.5, with $\gamma = 1.0$ corresponding to the classic NFW profile, but in our analysis we allow it to vary from 0.1–1.4.

Another popular profile that is easily parametrized in terms of the inner slope is the Einasto profile:

$$\rho(r) = \rho_s e^{-\frac{2}{\alpha}((\frac{r}{R_s})^\alpha - 1)}. \tag{4}$$

The proportionality constant is chosen to maintain the same slope and density at R_s as the NFW profile. Although the parameter α does not exactly correspond to the inner log slope, it does control the extent to which the profile is concentrated toward the center, with greater concentrations at smaller α. We therefore consider both Einasto and NFW profiles in our analysis, using γ and α to control how cuspy the profile is.

The ICS and bremsstrahlung components, particularly the ICS, have previously been found to contribute significantly to the signal, dominating it at lower energies ($E \lesssim 1$ GeV) [6]. This is especially true for gamma rays originating near or in the galactic disk [7,8]. This is due to the b-quark products decaying to high energy electrons and positrons, which in turn propagate through the interstellar medium and upscatter photons into the GeV range.

For the ICS and bremsstrahlung predictions, we use simulations to account for the propagation of decay products through the Milky Way and the distribution of gas and photons. We use the DRAGON code [24] to simulate the injection and propagation of high-energy electrons from DM annihilation, and the GAMMASKY program to compute the ICS and bremsstrahlung contributions resulting from these cosmic rays. GAMMASKY is as yet unreleased, though some results have been given [25]. GAMMASKY implements GALPROP in the calculation of photon production and upscattering along the line of sight.

The magnitude of the ICS component is highly model dependent. In the interest of consistency with previous work, we use the model parameters—describing the galactic magnetic field strength and shape and the galactic diffusion model used to compute the resulting inverse Compton scattering rates—adopted in Ref. [6], labeled Model F, which is found to perform particularly well in explaining the GCE signal. This results in an ICS component of the same magnitude as that found by the authors. We compare the results for a range of dark matter masses

[1]Measurements of the local dark matter density vary greatly, but tend to range from 0.2–0.5 GeV cm^{-3} [22]. Some analyses, however, indicate even larger values of up to 0.5–0.7 GeV cm^{-3} [23]. We adopt the value $\rho_\odot = 0.40$ GeV cm^{-3} in part to ease comparison with the results of Calore *et al.* [6]. Adopting a larger value for the local dark matter density would have the effect of easing the limits on the dwarf spheroidal galaxies by decreasing the best-fit annihilation cross section required to produce the purported GCE signal.

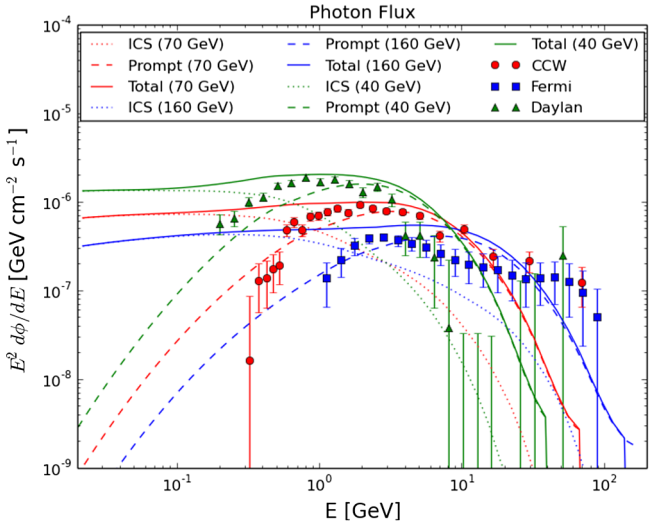

FIG. 1. Example of a simulated GCE signal (NFW profile, $\gamma_{\rm MW} = 1$) compared to that observed in Ref. [6] (red), Ref. [7] (green), and Ref. [8] (blue). The simulated signal is shown for the individual best-fit values in Table I. The spectra are masked to include only the region of interest considered in each data set ($2° < |b| < 20°$ and $|l| < 20°$, $1° < |b| < 20°$ and $|l| < 20°$, and $15° \times 15°$, respectively).

(20 GeV $\leq m_\chi \leq$ 200 GeV) to the GCE signals estimated in Refs. [6–8], as shown in Fig. 1.

We compare our predicted spectra to those observed in Refs. [6–8] by minimizing the χ^2 in the $\langle\sigma v\rangle$-m_χ plane to determine the best-fit values for both. For the first Ref. [6], we use the full covariance matrix; for the other two data sets, the published fluxes and error bars are used. Our results agree with those found in the original Refs. [6,7], and in Refs. [9,19] for each data set, though we find the best-fit mass to be slightly higher than Calore *et al.*

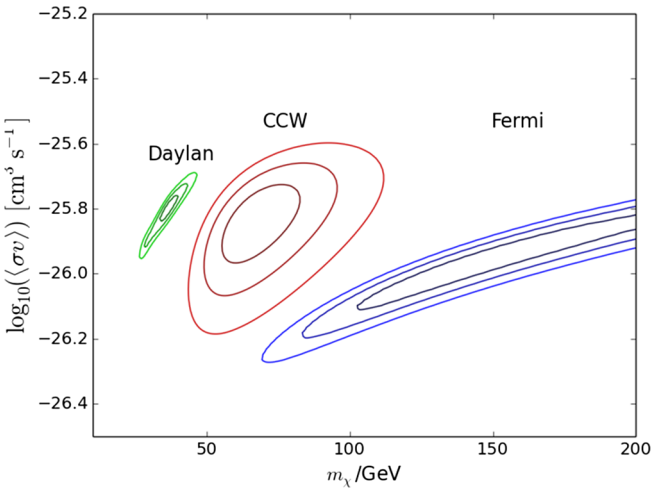

FIG. 2. Example of best-fit χ^2 1σ, 2σ, and 3σ contours for Ref. [6] (red), Ref. [7] (green), and Ref. [8] (blue). This example is for an NFW profile, $\gamma_{\rm MW} = 1$.

TABLE I. Best-fit values found for $\gamma_{\rm MW} = 1$.

Data set	$\langle\sigma v\rangle$[cm^3 s^{-1}]	m_χ[GeV]
CCW	1.5×10^{-26}	70
Fermi	1.3×10^{-26}	160
Daylan	1.7×10^{-26}	40

(70 GeV in our analysis, as opposed to 50 GeV). All found a best-fit cross section of approximately $\langle\sigma v\rangle = 1.7 \times 10^{-26}$ cm^3 s^{-1}.

Figure 2 shows the best-fit regions for $\gamma_{\rm MW} = 1$, showing the 1σ, 2σ, and 3σ confidence intervals generated by minimizing the χ^2 and creating contours at $\chi^2_{\rm min} + 2.30$, $+6.18$, and $+11.93$. This gives us our best-fit values which we will adopt when placing limits on the dwarf galaxy profiles. An example, for $\gamma_{\rm MW} = 1$, is shown in Table I.

III. THE DWARF SPHEROIDAL *J*-FACTORS

Given the assumption that the GCE signal is indeed the result of annihilating dark matter, our adopted values can be used to place constraints on the density profiles of dwarf spheroidal galaxies. We once again assume an NFW or Einasto profile, allowing the parameters $\gamma_{\rm dpsh}$ and $\alpha_{\rm dsph}$ to range from 0.1–1.2 and 0.01–1.0, respectively. In all cases the region of interest $\Delta\Omega$ is taken to be the entire sky in the integration. Observations of the gamma-ray flux from the dwarf spheroidals by Fermi-LAT use a $10° \times 10°$ region of interest [26]. Due to the small angular size of dwarf spheroidals (with an angular size less than 1 degree) this is large enough to be indistinguishable from the entire sky.

The exact halo parameters R_s and ρ_s of the dwarf spheroidals are not well known for either profile. Given the difficulty of measuring a large enough population of stars in the galaxies combined with the fact that they are very dark-matter dominated, stellar kinematic surveys tend to give us a view of the profiles of only the innermost regions of many dwarf spheroidals. Furthermore, these parameters themselves depend on the shape of the profile assumed; a given dwarf spheroidal will have different values for its characteristic radius and density depending on what value of $\gamma_{\rm dsph}$ or $\alpha_{\rm dsph}$ is chosen. We therefore derive best-fit parameters for individual values of $\gamma_{\rm dsph}$ and $\alpha_{\rm dsph}$ using the maximum likelihood method described in the Appendix, using stellar kinematic data from the 18 dwarf spheroidals for which data was available [27–35].

We see from the Appendix that varying the inner slope from $\gamma = 1.0$ to $\gamma = 0.2$ results in approximately an average reduction of 30% in the *J*-factor. This is twice as large as the 15% reduction found in the original Fermi-LAT dwarf spheroidal analysis [36], but in line with that found in the later analysis based on six years of Fermi-LAT data where a 20–40% difference was found [26]. Notably, however, large reductions are found for several dwarf

spheroidals with particularly large J-factors; for dwarf spheroidals with $J_{\rm NFW} > 19.0$ the average reduction is 40%. For the Einasto profile the difference is even more marked, with an average reduction of 70% from $\alpha = 0.2$ to $\alpha = 1.0$.

With our adopted value for the annihilation cross section from the fit to the GCE data, we can find the expected signal from any individual dwarf galaxy as a function of the dark matter mass m_χ using Eq. (2). Note that we only consider the prompt signal for dwarf spheroidal galaxies as they are much cleaner environments and therefore have negligible contributions from inverse Compton scattering or bremsstrahlung radiation.

The Fermi-LAT Collaboration has released the upper limits on the observed flux from a large number of Milky Way dwarf spheroidal galaxies based on six years of observation [26]. We compare our simulated observed flux to these reported limits, assuming an observed flux of 0 and taking their 95% C.L. limit as twice the 1σ deviation. Computing the χ^2 of our simulations versus their observations, we obtain a 95% C.L. constraint on the halo parameters as a function of mass by finding the contour along which $\chi^2 = \chi^2_{\rm min} + 6.18$. The resulting constraints are shown in Fig. 3. An upper limit can also be placed on the dark matter annihilation cross section $\langle\sigma v\rangle$ in the same manner. This upper limit is claimed to be in tension with the observed GCE flux [19]. In Fig. 5 we demonstrate the reduction of this limit as γ and α are varied.

In the analysis described so far, we have assumed $\gamma_{\rm MW} = 1.0$. If a smaller inner slope were chosen, we would expect an increase in the best-fit annihilation cross section

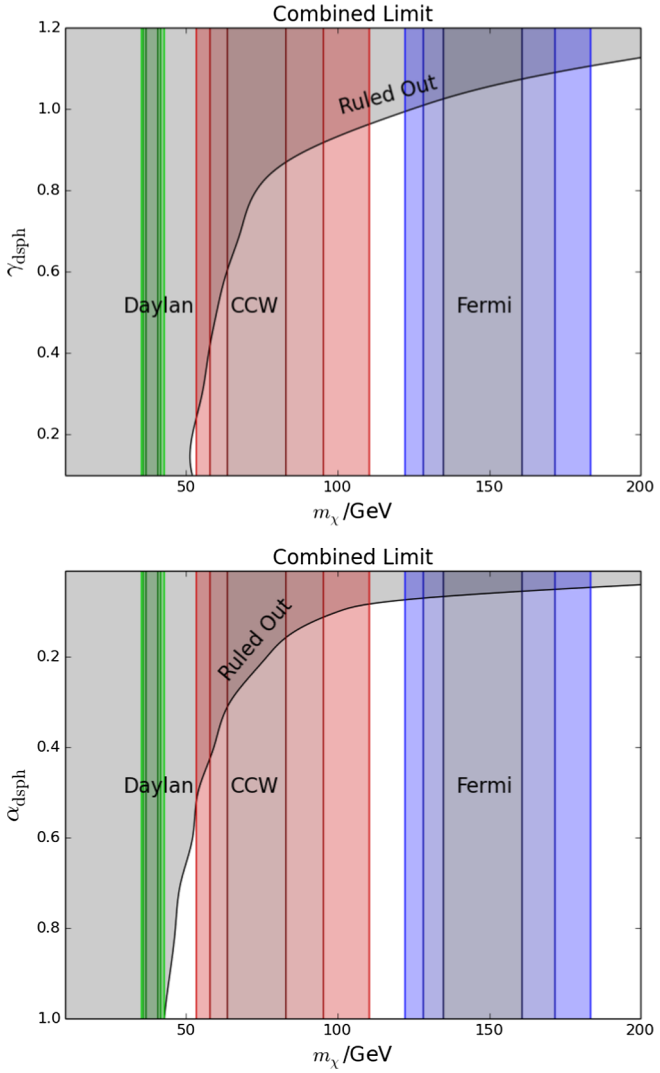

FIG. 3. 95% C.L. constraints on $\gamma_{\rm dsph}$ and $\alpha_{\rm dsph}$ for the generalized NFW (top) and Einasto (bottom) profiles, respectively. The best-fit contours for the fit to the GCE are shown in red [6], green [7], and blue [8]. We assume $\gamma_{\rm MW} = 1.0$ and $\langle\sigma v\rangle = 1.7 \times 10^{-26}$ cm^3 s^{-1}.

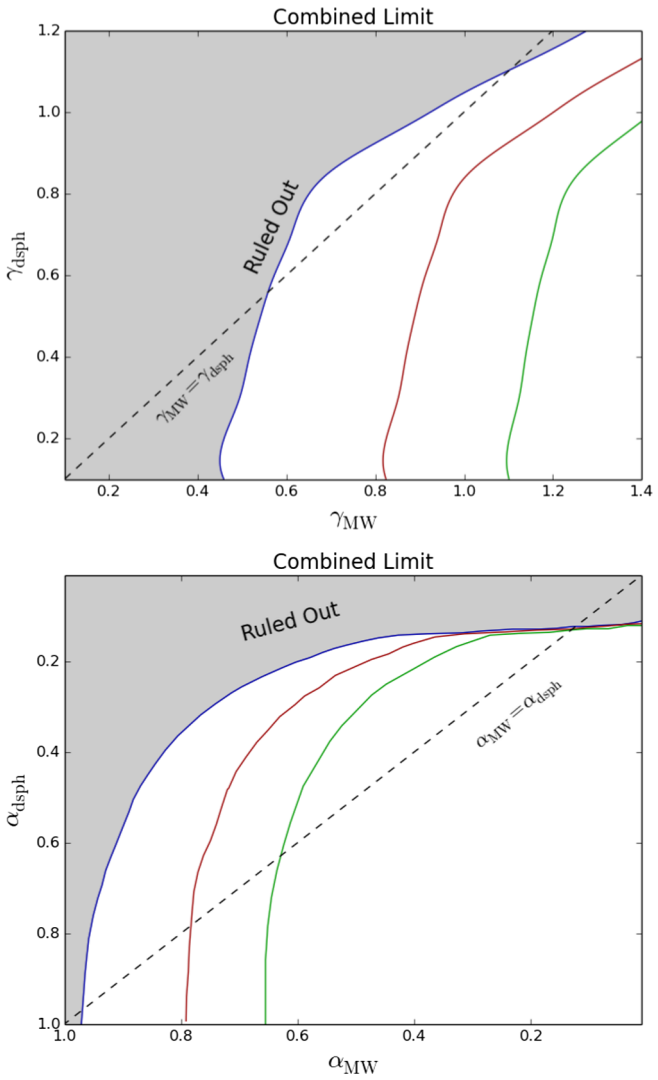

FIG. 4. 95% C.L. constraints on γ for both the Milky Way and the dwarf spheroidals. The signals are calculated for the individual best-fit masses and annihilation cross sections for each of the three data sets, as shown in Fig. 2.

for the signal. This would lead to correspondingly more stringent constraints on the dwarf spheroidals. We therefore repeat the calculation for several values of $\gamma_{\rm MW}$, as well as for Einasto profiles with the parameter $\alpha_{\rm MW}$ to produce constraints in the $\gamma_{\rm dsph}$-$\gamma_{\rm MW}$ and $\alpha_{\rm dsph}$-$\alpha_{\rm MW}$ planes, shown in Fig. 4.

IV. COMPARISON TO SIMULATIONS AND OBSERVATION

It has long been suspected that there is a discrepancy between the observed profiles of dwarf galaxies and those produced in CDM-only simulations. For a review of observational evidence and evidence from numerical simulations, see Ref. [37]. Early attempts to fit the observational data to an analytic profile [38,39] showed that dwarf galaxies are well characterized as having a constant density core ($\gamma = 0$) following an isothermal profile:

$$\rho_I = \frac{\rho_0}{1 + (r/R_C)^2}, \tag{5}$$

where ρ_0 is the central density and R_C is the core radius. A variation on the isothermal profile, the Burkert profile [40] was later introduced to account for observations indicating that the density falls off as r^{-3} at large radii:

$$\rho_B = \frac{\rho_0}{(1 + r/R_C)(1 + (r/R_C)^2)}. \tag{6}$$

Numerous other groups have found evidence for cored (rather than cuspy) halos in dwarf galaxies [41–45]

Few studies have presented a numerical best-fit value for the inner slope; instead, they have typically compared the NFW ($\gamma = 1$) model to an isothermal or Burkert profile ($\gamma = 0$). Those that did (several examples of which are listed below) tended to find values of $\gamma \sim 0.2$. Spekkens *et al.* [46] have derived density profiles for 165 low-mass galaxies including dwarf galaxies based on their rotation curves to find median inner slopes of $\gamma = 0.22 \pm 0.08$ to 0.28 ± 0.06 depending on the subsample considered.

Numerical simulations of CDM halos, on the other hand, have typically found values of the inner slope greater than $\gamma = 1$. Early numerical simulations of CDM halos were well characterized by the NFW profile of Eq. (3) with $\gamma \sim 1$ [47–49] for halos of all sizes. Others pointed towards an even steeper slope of $\gamma \sim 1.5$ [50,51] or an intermediate value of $\gamma \sim 1.2$ [52]. Despite this variation, there is general agreement that pure CDM simulations result in inner slopes of $\gamma \geq 1$.

Some simulations instead found that the slope continues to become more shallow at smaller radii but does not converge [53,54]. The Einasto profile (4) [55,56] parametrizes this kind of behavior. It describes a cored profile at large values of α and becomes cuspier for small values of order 0.1. The authors of Ref. [57] found that CDM simulations are well described by $\alpha \approx 0.17$, which even at $r/r_s = 10^{-3}$ provide a slope of $\gamma \sim 1$, and therefore for our purposes represents a cuspy profile.

It is clear that our results for the inner slopes of dwarf spheroidal halos, while compatible with observation, are not compatible with traditional CDM simulations. Our results favor values of $\gamma_{\rm dsph} < 1.0$. They also favor $\gamma_{\rm dsph} < \gamma_{\rm MW}$, which would suggest that the inner slope of the Milky Way's profile is steeper than that of dwarf spheroidals.

V. DISCUSSION

The core/cusp controversy is by no means new, and Ref. [58] reviewed it in great detail. Many mechanisms have been proposed through which baryonic matter can have a feedback effect on the dark matter halo in the hopes of giving a more cored halo, but the results have been mixed. These mechanisms include rotating bars [59] (however, later studies argued that this might actually have the opposite effect [60]) and the heating of cusps by dynamical friction [61–63] (however, again, others found that this process is insufficient to explain cored profiles [64]). Another possibility is feedback from supernovae [65,66]; in these simulations, repeated feedback from supernovae can turn a cusp into a core. Although viable baryonic mechanisms have been proposed to explain the discrepancy, its ultimate source remains an open question.

Although the standard CDM paradigm is difficult to render consistent with cored profiles, some dark matter models address this issue. Models of warm dark matter (WDM) such as sterile neutrinos rely on the particles having large velocities during structure formation, giving them a free-streaming length with a scale similar to galaxies. This smooths out density fluctuations on scales less than the free-streaming length, and is borne out in simulations of WDM halos, giving dwarf-sized halos a more cored profile [67–72]. The authors of Ref. [73] compared CDM and WDM simulations and found $\gamma =$ 1.18–1.46 for CDM and $\gamma = 0.25$–0.66 for WDM. It should be noted, however, that WDM faces many challenges, including conflict with the small-scale power spectrum [74], tension with strong-lens system observations (which show evidence for a larger subhalo population than would be produced by WDM [75]), and the fact that recent conservative estimates of the number of dwarf galaxies in the Milky Way restrict the WDM mass to $m_\chi \gtrsim 4$ keV, and may even restrict it to $m_\chi \gtrsim 8$ keV in the near future [76]. There are also challenges from observations of the Lyman-α forest which set a lower limit on the dark matter mass of a few keV [77,78]. These requirements may be inconsistent with the formation of sizable cores, which requires WDM masses of $m_\chi \lesssim 1$–2 keV [70].

Another solution to the cusp-core problem is self-interacting dark matter (SIDM), in which cold dark matter

has weak-scale interactions or no interactions at all with baryonic matter but a large self-interaction cross section. When the scattering cross section is of the order $\sigma/m_\chi \sim 0.1$–$1\ \mathrm{cm}^2\,\mathrm{g}^{-1}$, dark matter halos naturally form cores [79–81].

An interesting possibility is that of dark matter self-interacting through a light mediator. This results in a scattering cross section inversely proportional to velocity, causing greater self-interactions in dwarf galaxies than in galaxies or clusters [82]. For some choices of parameters, the cross section can be up to 100 times greater at velocities typically found in dwarf galaxies than for larger galaxies, which allows cored profiles to form for dwarfs but not for larger halos. These results correspond well to those presented here: the dwarf spheroidal halos are constrained to be more cored than that of the Milky Way. This "dark force" scattering can be further enhanced at dwarf-scale velocities by resonances, and the coupling can even be chosen such that the correct relic density is reproduced [83–85], though the simplest s-wave models are ruled out by cosmic microwave background constraints [86].

As WDM and SIDM are able to create cored halos, our results are consistent with these models which depart from the traditional CDM model. This implies that the GCE, if it does prove to originate from annihilating dark matter, would provide evidence in favor of these non-CDM cosmologies.

VI. CONCLUSIONS

We have presented constraints on the density profiles of dwarf spheroidal galaxy dark matter halos under the assumption that the reported Galactic Center excess is due to annihilating dark matter. As there is currently tension between dark matter explanations of the GCE and observations of dwarf spheroidal galaxies (which do not exhibit any discernible excess), we can make this assumption and work backwards to determine the characteristics a dwarf spheroidal galaxy's profile would need to satisfy in order to be consistent with the signal.

In the process of computing these constraints, we have determined the best-fit characteristic radii and densities of 18 dwarf spheroidal galaxies for various possible NFW and Einasto profile slopes. This was accomplished by applying the log-likelihood method to stellar kinematic data. We found that choosing a cored profile over a cuspy one leads to a reduction in the J-factor of approximately 30–50% in most cases, though the reduction varies for each individual dwarf.

We found that more cored profiles are favored, and that the GCE is consistent with most observations of dwarf galaxies which show dwarf galaxies to be consistent with cored profiles. This could suggest that the GCE is more consistent with SIDM or WDM models than with the traditional CDM model.

ACKNOWLEDGMENTS

I would like to thank James Cline and Jonathan Cornell for their ideas and assistance in preparing and reviewing this work, and Wei Xue for the use of and assistance with the GammaSky program. I also thank Matthew Walker for helpful correspondence and Marla Geha for providing us with the stellar kinematic data for several dwarf galaxies through private correspondence. This work was done with the support of the McGill Space Institute and the Natural Sciences and Engineering Research Council of Canada.

APPENDIX: MAXIMUM LIKELIHOOD METHOD

We adopt the method of Geringer-Sameth *et al.* [87] to calculate the halo parameters using the maximum likelihood method. They argued that the velocity data sample a Gaussian distribution, and therefore adopted the likelihood [87]

$$L = \prod_{i=1}^{N} \frac{\exp\left[-\frac{1}{2}\frac{(u_i-\langle u\rangle)^2}{\delta_{u,i}^2+\sigma^2(R_i)}\right]}{(2\pi)^{1/2}(\delta_{u,i}^2+\sigma^2(R_i))^{1/2}}, \tag{A1}$$

where u_i and $\delta_{u,i}$ are the observed line-of-sight velocity and uncertainty, $\langle u\rangle$ is the mean velocity of the dwarf, and $\sigma^2(R_i)$ is the velocity dispersion at the projected position of the observed star.

The velocity dispersion is a model-dependent quantity, and has the form [88]

$$\sigma^2(R) = \frac{2G}{\Sigma(R)}\int_R^\infty \frac{v(s)M(s)}{s^2}\sqrt{s^2-R^2}\,ds \tag{A2}$$

for an isotropic halo (where the parameter describing the velocity anisotropy, β_a, has been set to 0). $M(r)$ is the mass contained within the given radius, and $v(r)$ and $\Sigma(R)$ are the stellar density and luminosity profiles, respectively.

For a halo in which stars are distributed according to a Plummer profile [87], the ratio of these profiles is given by

$$\frac{v(r)}{\Sigma(R)} = \frac{3}{4r_{1/2}}\frac{1}{\sqrt{1+r^2/r_{1/2}^2}}, \tag{A3}$$

where $r_{1/2}$ is the half-light radius.

Note that we make two assumptions about the stellar profiles: the first is that the Plummer profile accurately describes the stellar distribution, and the second is that the velocity anisotropy is 0. For any given dwarf spheroidal both of these assumptions will be violated to some degree. The Plummer profile, however, is generally recognized as a good fit to the stellar distributions of dwarf spheroidals [89–92]. In the analysis of Ref. [87], most dwarf

TABLE II. Best-fit NFW parameters for various values of $\gamma_{\rm dsph}$. Typical values of the relative uncertainties are ∼10% for R_s and ∼15% for ρ_s.

	$\gamma = 0.2$		$\gamma = 0.4$		$\gamma = 0.6$		$\gamma = 0.8$		$\gamma = 1.0$[b]		
Dwarf Galaxy	R_s [kpc]	ρ_s [GeV/cm^3]	R_s	ρ_s	R_s	ρ_s	R_s	ρ_s	R_s	ρ_s	References
Carina	0.68	2.4	0.79	1.6	0.93	1.0	1.1	0.6	1.4	0.32	[27]
Draco	1.4	4.7	1.8	2.7	2.6	1.4	4.6	0.49	–	–	[28]
Fornax	0.66	6.6	0.74	4.8	0.84	3.3	0.98	2.1	1.2	1.3	[27]
Leo I	1.1	3.4	1.4	2.1	1.9	1.2	2.8	0.53	5.5	0.15	[29]
Leo II	1.1	3.1	1.4	1.9	1.9	1.1	2.8	0.48	6.1	0.13	[30]
Sculptor	0.57	6.6	0.65	4.5	0.76	2.9	0.92	1.8	1.2	0.98	[27]
Sextans	0.59	3.5	0.68	2.4	0.8	1.6	0.97	0.94	1.2	0.52	[27]
Bootes I	1.7	6.4	2.4	3.6	3.9	1.6	36	0.13	–	–	[31]
Hercules	1.0	0.62	1.2	0.39	1.6	0.22	2.2	0.11	3.7	0.039	[32][a]
Leo V	2.0	1.3	2.8	0.73	5.5	0.3	40	0.012	–	–	[33]
Segue 1	1.1	4.4	1.4	2.7	1.9	1.5	2.8	0.67	6.4	0.17	[34]
Segue 2	1.4	4.9	1.8	2.9	2.6	1.5	4.9	0.54	–	–	[35]
Canes Venatici I	1.9	1.1	2.6	0.59	4.3	0.26	16	0.047	–	–	[32][a]
Canes Venatici II	1.5	5.1	2	4.1	2.9	2	6.3	0.66	–	–	[32][a]
Coma Berenices	1.4	6	1.9	3.5	2.7	1.8	5.4	0.62	–	–	[32][a]
Leo T[c]	0.076	210	0.088	140	0.1	86	0.13	50	0.16	27	[32][a]
UrsaMajor I	0.16	30	0.18	21	0.21	14	0.25	8.3	0.31	4.8	[32][a]
UrsaMajor II	1.6	3.6	2.1	2.1	3.2	0.99	8	0.27	–	–	[32][a]

[a]Unpublished; provided by private correspondence.
[b]For missing data, see explanation in text.
[c]Due to lack of FERMI-LAT data, this dwarf is excluded from constraints on γ.

TABLE III. Best-fit Einasto parameters for various values of $\alpha_{\rm dsph}$. Typical values of the relative uncertainties are ∼10% for R_s and ∼15% for ρ_s.

	$\alpha = 0.2$		$\alpha = 0.4$		$\alpha = 0.6$		$\alpha = 0.8$		$\alpha = 1.0$		
Dwarf Galaxy	R_s [kpc]	ρ_s [GeV/cm^3]	R_s	ρ_s	R_s	ρ_s	R_s	ρ_s	R_s	ρ_s	References
Carina	1.6	0.061	1.3	0.11	1.2	0.16	1.2	0.20	1.1	0.24	[27]
Draco	15	0.016	2.9	0.19	1.8	0.44	1.4	0.67	1.2	0.85	[28]
Fornax	1.1	0.34	1.4	0.24	1.5	0.21	1.6	0.2	1.7	0.19	[27]
Leo I	8.0	0.02	2.2	0.16	1.5	0.3	1.2	0.41	1.1	0.48	[29]
Leo II	8.2	0.018	2.2	0.14	1.5	0.27	1.2	0.36	1.1	0.42	[30]
Sculptor	1.3	0.19	1.2	0.24	1.2	0.26	1.2	0.28	1.2	0.29	[27]
Sextans	1.3	0.11	1.2	0.14	1.2	0.15	1.2	0.16	1.2	0.17	[27]
Bootes I	38	0.013	4.1	0.24	2.1	0.59	1.6	0.88	1.3	1.1	[31]
Hercules	5.6	0.0048	1.8	0.03	1.3	0.052	1.1	0.068	1.5	0.62	[32][a]
Leo V	63	0.0021	5.1	0.047	2.4	0.12	1.7	0.18	1.4	0.23	[33]
Segue 1	8.7	0.025	2.2	0.2	1.4	0.38	1.2	0.51	1.1	0.58	[34]
Segue 2	17	0.017	3	0.2	1.7	0.52	1.4	0.69	1.2	0.8	[35]
Canes Venatici I	40	0.002	4.5	0.039	2.3	0.1	1.7	0.16	1.4	0.2	[32][a]
Canes Venatici II	22	0.021	3.3	0.28	1.8	0.48	1.4	0.65	1.3	0.76	[32][a]
Coma Berenices	19	0.019	3.1	0.25	1.8	0.54	1.4	0.77	1.2	0.92	[32]
Leo T[c]	0.16	6.2	0.16	7.3	0.17	7.6	0.18	8.2	0.18	9.4	[32][a]
UrsaMajor I	0.32	1.1	0.35	0.96	0.41	0.72	0.47	0.56	0.52	0.46	[32][a]
UrsaMajor II	26	0.0092	3.5	0.14	1.9	0.33	1.5	0.48	1.3	0.59	[32][a]

[a]Unpublished; provided by private correspondence.
[c]Due to lack of FERMI-LAT data, this dwarf is excluded from constraints on γ.

TABLE IV. J-factors derived from best-fit parameters for various values of $\gamma_{\rm dsph}$.

	$\gamma = 0.2 = \alpha$		$\gamma = 0.6 = \alpha$		$\gamma = 1.0 = \alpha$		$J_{\gamma=0.2}/J_{\gamma=1.0}$	$J_{\alpha=1.0}/J_{\alpha=0.2}$	
Dwarf Galaxy	$J_{\rm NFW}$	$J_{\rm Einasto}$	$J_{\rm NFW}$	$J_{\rm Einasto}$	$J_{\rm NFW}$	$J_{\rm Einasto}$	NFW	Einasto	References
Carina	17.4	17.6	17.4	17.6	17.4	17.7	0.844	1.3	[27]
Draco	18.8	19.6	18.9	19.2	18.9	19.2	0.924	0.403	[28]
Fornax	18	18.3	18	17.9	18.1	17.8	0.711	0.32	[27]
Leo I	17.6	17.9	17.7	17.6	17.7	17.6	0.843	0.443	[29]
Leo II	17.6	17.9	17.6	17.6	17.7	17.5	0.795	0.387	[30]
Sculptor	18.2	18.4	18.2	18.2	18.3	18.1	0.777	0.539	[27]
Sextans	17.7	17.9	17.7	17.7	17.8	17.7	0.771	0.524	[27]
Bootes I	19.4	20.7	19.4	19.8	19.4	19.7	0.77	0.0859	[31]
Hercules	16.5	16.8	16.5	16.5	16.5	18.7	0.858	91.4[b]	[32][a]
Leo V	17.7	19	17.8	17.8	16.8	18.5	7.94[b]	0.331	[33]
Segue 1	19	20.3	19.2	19.9	19.3	19.8	0.507	0.308	[34]
Segue 2	19.1	20.5	19.3	20	19.4	19.8	0.555	0.215	[35]
Canes Venatici I	17.3	18.2	17.4	17.4	17.5	17.2	0.694	0.12	[32][a]
Canes Venatici II	18.6	19.7	19	18.7	18.9	18.5	0.567	0.0739	[32][a]
Coma Berenices	19.3	20.5	19.4	19.9	19.5	19.8	0.6	0.165	[32][a]
Leo T[c]	17	16.9	17	14.7	17	13.8	1.15	0.000671[b]	[32][a]
UrsaMajor I	17.8	18	17.9	17.5	17.9	17.4	0.842	0.238	[32][a]
UrsaMajor II	19	20.6	19.1	19.8	19.1	19.7	0.747	0.132	[32][a]

[a]Unpublished; provided by private correspondence.
[b]See explanation in text.
[c]Due to lack of FERMI-LAT data, this dwarf is excluded from constraints on γ.

spheroidals were found to have nearly isotropic orbital velocities. We therefore adopt the simplifying assumption of $\beta_a = 0$ for all dwarf spheroidals.

The mass contained within a given radius is attained by integrating the chosen density profile:

$$M(s) = \int_0^s 4\pi r^2 \rho_s(r, R_s, \rho_s, \gamma) dr. \tag{A4}$$

For each dwarf spheroidal we minimize the negative log likelihood for $0.1 \leq \gamma \leq 1.2$ and again for $0.1 \leq \alpha \leq 1.0$ (for the NFW and Einasto profiles, respectively) over the parameters R_s and ρ_s. This is accomplished using the downhill simplex method over the two parameters. The best-fit values of R_s and ρ_s are shown in Table II for several values of γ and in Table III for α, the Einasto profile parameter.

Best-fit values are not available for some dwarf galaxies for $\gamma = 1.0$ (or greater). The likelihood in these cases approaches its maximum value only as $r_s \to \infty$ and $\rho_s \to \infty$. This is due to the nature of the NFW profile, which has its shallowest log slope at $r = 0$, with the slope becoming steeper at greater distances. In these cases, therefore, the slope $\gamma = 1.0$ is inconsistent with the stellar kinematic data. In these cases the fit can always be made better by increasing r_s to grant a smaller log slope (approaching a uniform log slope of 1.0) and reducing the density to compensate.

Typical relative errors on R_s are approximately $\sim \pm 10\%$, while those on ρ_s are somewhat larger ($\sim \pm 15\%$). These are found by varying each parameter from the best fit until the criteria $\Delta \ln \mathcal{L} = 2.6/\ln 2$ is satisfied. The fits are not good enough to discriminate between values of γ or α, with the log likelihood varying by only $\Delta \ln \mathcal{L} \sim 0.5$ for all dwarf spheroidals between $0.1 \leq \gamma \leq 1.2$ and $0.1 \leq \alpha \leq 1.0$.

In Table IV we present the J-factors corresponding to the best-fit halo parameters for γ, $\alpha = 0.2$, 0.6, and 1.0, and Fig. 5 shows the corresponding effect on the upper limit on the annihilation cross section. Note that even in the cases of $\gamma = 1.0$ where the halo parameters cannot be found, the J-factor is nonetheless convergent. We also demonstrate the reduction of the J-factors for both profiles as the inner slope is changed. For the NFW profiles, $J_{\gamma=0.2}/J_{\gamma=1.0} \sim 0.7$ on average, and in Einasto profiles the difference is even more marked with $J_{\alpha=1.0}/J_{\gamma=0.2} \sim 0.4$. A few of the dwarf spheroidals show an opposite trend, with the J-factor increasing as the profile is made more cored, notably Hercules (for the Einasto profile) with $J_{\alpha=1.0}/J_{\gamma=0.2} = 91.4$ and Leo V (for the NFW profile) with $J_{\gamma=0.2}/J_{\gamma=1.0} = 7.94$. Little stellar kinematical data exists for Hercules and Leo V, and our analyses are therefore based on very few data points, which could explain this discrepancy. The same is true of Leo T, which displays the opposite behavior with an unrealistically large decrease in the J-factor.

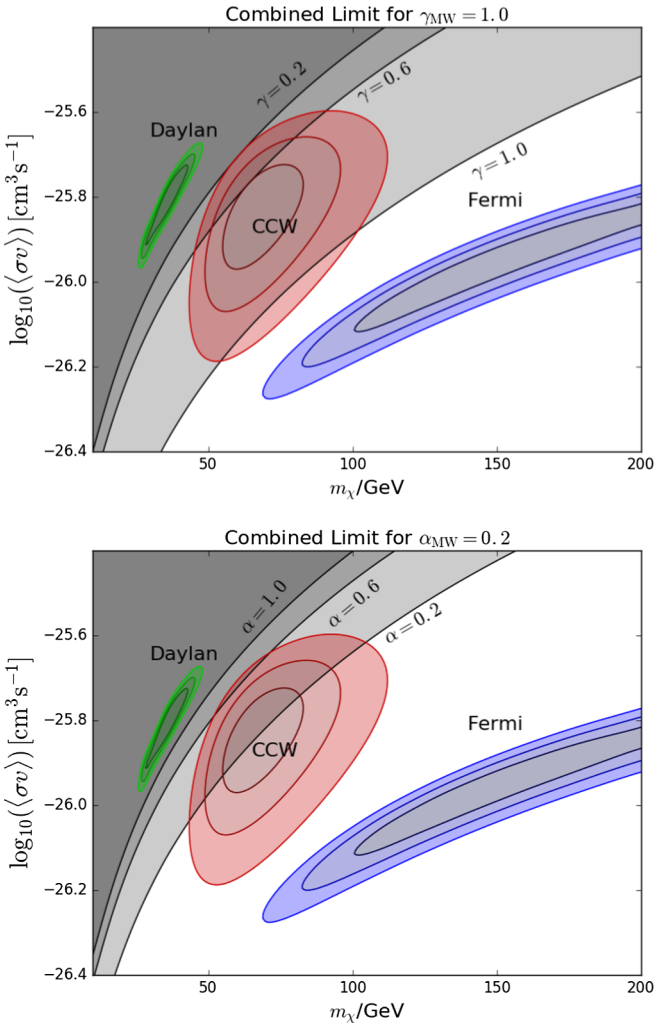

FIG. 5. As in Fig. 2, but also shown is the combined 95% C.L. upper limit on $\langle\sigma v\rangle$ from the dwarf spheroidals. This is shown for several values of γ and α, demonstrating how the limit is weakened when considering more cored profiles (smaller γ or larger α).

[1] L. Goodenough and D. Hooper, arXiv:0910.2998.
[2] D. Hooper and L. Goodenough, Phys. Lett. B **697**, 412 (2011).
[3] D. Hooper and T. Linden, Phys. Rev. D **84**, 123005 (2011).
[4] K. N. Abazajian and M. Kaplinghat, Phys. Rev. D **86**, 083511 (2012); **87**, 129902(E) (2013).
[5] B. Zhou, Y.-F. Liang, X. Huang, X. Li, Y.-Z. Fan, L. Feng, and J. Chang, Phys. Rev. D **91**, 123010 (2015).
[6] F. Calore, I. Cholis, and C. Weniger, J. Cosmol. Astropart. Phys. 03 (2015) 038.
[7] T. Daylan, D. P. Finkbeiner, D. Hooper, T. Linden, S. K. N. Portillo, N. L. Rodd, and T. R. Slatyer, Phys. Dark Universe **12**, 1 (2016).
[8] M. Ajello *et al.* (Fermi-LAT Collaboration), Astrophys. J. **819**, 44 (2016).
[9] C. Karwin, S. Murgia, T. M. P. Tait, T. A. Porter, and P. Tanedo, Phys. Rev. D **95**, 103005 (2017).
[10] S. K. Lee, M. Lisanti, B. R. Safdi, T. R. Slatyer, and W. Xue, Phys. Rev. Lett. **116**, 051103 (2016).
[11] R. Bartels, S. Krishnamurthy, and C. Weniger, Phys. Rev. Lett. **116**, 051102 (2016).
[12] R. M. O'Leary, M. D. Kistler, M. Kerr, and J. Dexter, arXiv:1504.02477.
[13] T. Linden, Phys. Rev. D **93**, 063003 (2016).
[14] I. Cholis, D. Hooper, and T. Linden, J. Cosmol. Astropart. Phys. 06 (2015) 043.
[15] M. Ackermann *et al.* (Fermi-LAT Collaboration), Astrophys. J. **840**, 43 (2017).
[16] M. Ajello *et al.* (Fermi-LAT Collaboration), arXiv: 1705.00009.

[17] D. Haggard, C. Heinke, D. Hooper, and T. Linden, J. Cosmol. Astropart. Phys. 05 (2017) 056.
[18] M. Ackermann *et al.* (Fermi-LAT Collaboration), Phys. Rev. D **91**, 122002 (2015).
[19] K. N. Abazajian and R. E. Keeley, Phys. Rev. D **93**, 083514 (2016).
[20] M. Cirelli, G. Corcella, A. Hektor, G. Hütsi, M. Kadastik, P. Panci, M. Raidal, F. Sala, and A. Strumia, J. Cosmol. Astropart. Phys. 03 (2011) 051; 10 (2012) E01.
[21] P. Ciafaloni, D. Comelli, A. Riotto, F. Sala, A. Strumia, and A. Urbano, J. Cosmol. Astropart. Phys. 03 (2011) 019.
[22] J. I. Read, J. Phys. G **41**, 063101 (2014).
[23] B. Burch and R. Cowsik, Astrophys. J. **779**, 35 (2013).
[24] C. Evoli, D. Gaggero, D. Grasso, and L. Maccione, J. Cosmol. Astropart. Phys. 10 (2008) 018.
[25] G. Di Bernardo, C. Evoli, D. Gaggero, D. Grasso, and L. Maccione, J. Cosmol. Astropart. Phys. 03 (2013) 036.
[26] M. Ackermann *et al.* (Fermi-LAT Collaboration), Phys. Rev. Lett. **115**, 231301 (2015).
[27] M. G. Walker, M. Mateo, and E. Olszewski, Astron. J. **137**, 3100 (2009).
[28] M. G. Walker, E. W. Olszewski, and M. Mateo, Mon. Not. R. Astron. Soc. **448**, 2717 (2015).
[29] M. Mateo, E. W. Olszewski, and M. G. Walker, Astrophys. J. **675**, 201 (2008).
[30] A. Koch, J. T. Kleyna, M. I. Wilkinson, E. K. Grebel, G. F. Gilmore, N. W. Evans, R. F. G. Wyse, and D. R. Harbeck, Astron. J. **134**, 566 (2007).
[31] S. E. Koposov *et al.*, Astrophys. J. **736**, 146 (2011).
[32] J. D. Simon and M. Geha, Astrophys. J. **670**, 313 (2007).
[33] M. G. Walker, V. Belokurov, N. W. Evans, M. J. Irwin, M. Mateo, E. W. Olszewski, and G. Gilmore, Astrophys. J. **694**, L144 (2009).
[34] J. D. Simon *et al.*, Astrophys. J. **733**, 46 (2011).
[35] E. N. Kirby, M. Boylan-Kolchin, J. G. Cohen, M. Geha, J. S. Bullock, and M. Kaplinghat, Astrophys. J. **770**, 16 (2013).
[36] M. Ackermann *et al.* (Fermi-LAT Collaboration), Phys. Rev. D **89**, 042001 (2014).
[37] W. J. G. de Blok, Adv. Astron. **2010**, 789293 (2010).
[38] B. Moore, Nature (London) **370**, 629 (1994).
[39] R. A. Flores and J. R. Primack, Astrophys. J. **427**, L1 (1994).
[40] A. Burkert, IAU Symp. **171**, 175 (1996) Astrophys. J. **447**, L25 (1995).
[41] A. Burkert and J. Silk, Astrophys. J. **488**, L55 (1997).
[42] F. C. van den Bosch and R. A. Swaters, Mon. Not. R. Astron. Soc. **325**, 1017 (2001).
[43] P. Salucci, F. Walter, and A. Borriello, Astron. Astrophys. **409**, 53 (2003).
[44] G. Gentile, P. Salucci, U. Klein, and G. L. Granato, Mon. Not. R. Astron. Soc. **375**, 199 (2007).
[45] R. Cowsik, K. Wagoner, E. Berti, and A. Sircar, Astrophys. J. **699**, 1389 (2009).
[46] K. Spekkens and R. Giovanelli, Astron. J. **129**, 2119 (2005).
[47] J. Dubinski and R. G. Carlberg, Astrophys. J. **378**, 496 (1991).
[48] J. F. Navarro, C. S. Frenk, and S. D. M. White, Astrophys. J. **490**, 493 (1997).
[49] P. Colin, A. Klypin, O. Valenzuela, and S. Gottlober, Astrophys. J. **612**, 50 (2004).
[50] B. Moore, T. R. Quinn, F. Governato, J. Stadel, and G. Lake, Mon. Not. R. Astron. Soc. **310**, 1147 (1999).
[51] A. Klypin, A. V. Kravtsov, J. Bullock, and J. Primack, Astrophys. J. **554**, 903 (2001).
[52] J. Diemand, M. Zemp, B. Moore, J. Stadel, and M. Carollo, Mon. Not. R. Astron. Soc. **364**, 665 (2005).
[53] J. F. Navarro, E. Hayashi, C. Power, A. R. Jenkins, C. S. Frenk, S. D. M. White, V. Springel, J. Stadel, and T. R. Quinn, Mon. Not. R. Astron. Soc. **349**, 1039 (2004).
[54] E. Hayashi, J. F. Navarro, C. Power, A. Jenkins, C. S. Frenk, S. D. M. White, V. Springel, J. Stadel, and T. R. Quinn, Mon. Not. R. Astron. Soc. **355**, 794 (2004).
[55] D. Merritt, J. F. Navarro, A. Ludlow, and A. Jenkins, Astrophys. J. **624**, L85 (2005).
[56] A. W. Graham, D. Merritt, B. Moore, J. Diemand, and B. Terzic, Astron. J. **132**, 2701 (2006).
[57] J. F. Navarro, A. Ludlow, V. Springel, J. Wang, M. Vogelsberger, S. D. M. White, A. Jenkins, C. S. Frenk, and A. Helmi, Mon. Not. R. Astron. Soc. **402**, 21 (2010).
[58] D. H. Weinberg, J. S. Bullock, F. Governato, R. K. de Naray, and A. H. G. Peter, Proc. Natl. Acad. Sci. U.S.A. **112**, 12249 (2015).
[59] M. D. Weinberg and N. Katz, Astrophys. J. **580**, 627 (2002).
[60] J. Dubinski, I. Berentzen, and I. Shlosman, IAU Symp. **254**, 165 (2009).
[61] A. El-Zant, I. Shlosman, and Y. Hoffman, Astrophys. J. **560**, 636 (2001).
[62] C. Tonini and A. Lapi, Astrophys. J. **649**, 591 (2006).
[63] E. Romano-Diaz, I. Shlosman, Y. Hoffman, and C. Heller, Astrophys. J. **685**, L105 (2008).
[64] J. R. Jardel and J. A. Sellwood, Astrophys. J. **691**, 1300 (2009).
[65] A. Pontzen and F. Governato, Mon. Not. R. Astron. Soc. **421**, 3464 (2012).
[66] F. Governato, A. Zolotov, A. Pontzen, C. Christensen, S. H. Oh, A. M. Brooks, T. Quinn, S. Shen, and J. Wadsley, Mon. Not. Roy. Astron. Soc. **422**, 1231 (2012).
[67] V. Avila-Reese, P. Colin, O. Valenzuela, E. D'Onghia, and C. Firmani, Astrophys. J. **559**, 516 (2001).
[68] P. Colin, O. Valenzuela, and V. Avila-Reese, Astrophys. J. **673**, 203 (2008).
[69] R. M. Dunstan, K. N. Abazajian, E. Polisensky, and M. Ricotti, arXiv:1109.6291.
[70] A. V. Maccio, S. Paduroiu, D. Anderhalden, A. Schneider, and B. Moore, Mon. Not. R. Astron. Soc. **424**, 1105 (2012).
[71] A. Schneider, D. Anderhalden, A. Maccio, and J. Diemand, Mon. Not. R. Astron. Soc. **441**, L6 (2014).
[72] R. E. Angulo, O. Hahn, and T. Abel, Mon. Not. R. Astron. Soc. **434**, 3337 (2013).
[73] A. Gonzalez-Samaniego, V. Avila-Reese, and P. Colin, Astrophys. J. **819**, 101 (2016).
[74] E. Polisensky and M. Ricotti, Phys. Rev. D **83**, 043506 (2011).
[75] N. Dalal and C. S. Kochanek, Astrophys. J. **572**, 25 (2002).
[76] S. Y. Kim, A. H. G. Peter, and J. R. Hargis, arXiv:1711.06267.
[77] U. Seljak, A. Makarov, P. McDonald, and H. Trac, Phys. Rev. Lett. **97**, 191303 (2006).
[78] M. Viel, G. D. Becker, J. S. Bolton, M. G. Haehnelt, M. Rauch, and W. L. W. Sargent, Phys. Rev. Lett. **100**, 041304 (2008).

[79] D. N. Spergel and P. J. Steinhardt, Phys. Rev. Lett. **84**, 3760 (2000).
[80] M. Rocha, A. H. G. Peter, J. S. Bullock, M. Kaplinghat, S. Garrison-Kimmel, J. Oñorbe, and L. A. Moustakas, Mon. Not. R. Astron. Soc. **430**, 81 (2013).
[81] A. H. G. Peter, M. Rocha, J. S. Bullock, and M. Kaplinghat, Mon. Not. R. Astron. Soc. **430**, 105 (2013).
[82] A. Loeb and N. Weiner, Phys. Rev. Lett. **106**, 171302 (2011).
[83] S. Tulin, H.-B. Yu, and K. M. Zurek, Phys. Rev. Lett. **110**, 111301 (2013).
[84] S. Tulin, H.-B. Yu, and K. M. Zurek, Phys. Rev. D **87**, 115007 (2013).
[85] M. Kaplinghat, S. Tulin, and H.-B. Yu, Phys. Rev. Lett. **116**, 041302 (2016).
[86] T. Bringmann, F. Kahlhoefer, K. Schmidt-Hoberg, and P. Walia, Phys. Rev. Lett. **118**, 141802 (2017).
[87] A. Geringer-Sameth, S. M. Koushiappas, and M. Walker, Astrophys. J. **801**, 74 (2015).
[88] G. A. Mamon and E. L. Lokas, Mon. Not. R. Astron. Soc. **363**, 705 (2005); Mon. Not. Roy. Astron. Soc. **370**, 1582(E) (2006).
[89] M. Irwin and D. Hatzidimitriou, Mon. Not. R. Astron. Soc. **277**, 1354 (1995).
[90] S. Mashchenko, A. Sills, and H. M. P. Couchman, Astrophys. J. **640**, 252 (2006).
[91] M. G. Walker, M. Mateo, E. W. Olszewski, J. Peñarrubia, N. W. Evans, and G. Gilmore, Astrophys. J. **704**, 1274 (2009); **710**, 886 (2010).
[92] A. McConnachie and M. Irwin, Mon. Not. R. Astron. Soc. **365**, 1263 (2006).